Analyzing the role of *her1* 3'UTR cis-elements in *her1* post-transcriptional expression

Introduction

In vertebrates, segmentation is the process of patterning the mesoderm into repetitive sections called somites along the body axis during embryogenesis (Pais-de-Azevedo et al, 2018). Formed somites will differentiate into the mature axial skeleton, musculature, connective tissue, blood vessel, and muscles (Pais-de-Azevedo et al, 2018). Segmentation is regulated by a molecular oscillator called the segmentation clock, a network of oscillating genes expressed in the presomitic mesoderm (PSM) cells (Pais-de-Azevedo et al. 2018). The oscillating genes in the segmentation clock regulate somite formation, and the period of segmentation clock oscillation corresponds to the period of somite formation. Segmentation clock genes need to maintain their oscillatory expression so that embryos have a proper pattern of somite formation. In mouse embryos, segmentation clock gene *Hes7* knockout disrupts the *Hes7* oscillation, which leads to irregular somites and fused somites (Bessho et al, 2001).

The rhythmic expression of clock genes drives periodic boundary formation in the anterior PSM, and the period of clock gene expression is coincident with the period of somite formation which is different in different species (Gomez et al, 2008). In zebrafish, the period is 30 minutes, in mice, the period is 2 hours, and in chick, the period is 90 minutes (Gomez et al, 2008). The Delta-Notch signaling pathway is also involved in regulating the segmentation clock period (Herrgen et al, 2010). In the PSM, Delta-Notch signaling participates in cell-cell communication and synchronizes segmentation clock oscillations between PSM cells, therefore it is able to control the collected segmentation clock period in PSM cells (Herrgen et al, 2010). One of the genes that Delta-Notch signaling synchronizes between PSM cells is *Hes/her* gene, one of the core oscillators in segmentation. Delta-Notch signaling disruption leads to a longer segmentation clock period (Herrgen et al, 2010)

In the zebrafish embryo, *her1* and *her7* are core clock genes that encode basic Helix-Loop-Helix (bHLH) transcription factors. *her1*orthologs are also found in other vertebrate animals, suggesting that it is important during development (Palmeirim et al, 1997). Zebrafish *her1* and *her7* are expressed in an oscillating manner and oscillations are maintained through feedback inhibition in the PSM. *her1* operates in an auto-regulatory negative feedback loop, in which Her1 protein inhibits transcription of *her1* (Choorapoikayil et al, 2012, Dawson et al, 1995). After the *her1* gene is transcriptionally activated in a PSM cell, *her1* mRNA and, subsequently Her1 protein, are produced. As a transcriptional repressor, Her1 protein inhibits its own transcription (Kageyama et al, 2012). As a result, when Her1 protein level is high, *her1*

transcription is shut off, thus temporarily halting the production of mRNA and protein. The existing transcript and protein are rapidly degraded and decreasing levels of Her1 protein allow transcription to start again. Using this negative feedback system, the *her1* gene maintains oscillatory expression (Gajewski et al, 2003, Giudicelli et al, 2007). *her1* Knockout leads to defects in the anterior-most somite borders in the zebrafish embryo and disrupts the cyclic expression of *her1* (Choorapoikayil et al, 2012*). her1* is required for proper anterior somite formation while *her7* is required for posterior somite formation (Pais-de-Azevedo et al, 2018).

Since clock gene periodicity regulates somite formation, clock gene expression needs to be precisely regulated to maintain oscillations. To obtain a precise period, segmentation clock gene mRNA needs to be cleared during each cycle so that the segmentation clock gene can oscillate. Therefore, post-transcriptional control, including mRNA decay, is necessary for clock gene regulation. Understanding post-transcriptional control will reveal critical aspects of how the segmentation clock is regulated and how clock periodicity is maintained during somitogenesis. Previous studies using an inducible reporter system determined that the *her1* 3'UTR is necessary for the decay of reporter transcripts (Gallagher et al, 2017). The heat-shock inducible reporter transgene contains the heat shock promoter and Venus coding sequence and expression is induced after a brief heat shock at 37°C. The *her1* 3'UTR, and several variations, were appended to the Venus coding sequence to quantify whether it influenced reporter mRNA decay. At various times post-heat shock, mRNA abundance was measured via in situ hybridization and qPCR analysis. The results indicated that the reporter transcript fused with full-length *her1* 3'UTR was rapidly degraded, indicating that the reporter mRNA was unstable (Gallagher et al, 2017). Deletion analysis using reporter transcripts fused to different portions of the *her1* 3'UTR indicated that a Pumilio Response Element (PRE) and an AU-rich element (ARE) located in the last half of the 3'UTR were required for the reporter transcripts degradation (Tietz et al., 2020). Mutation of either the PRE or ARE moderately increased reporter transcript half-life and stabilized reporter transcripts, whereas mutation of both the ARE and PRE sites significantly increased the half-life of reporter transcripts (Tietz et al., 2020). The results show that the ARE and PRE are both required for rapid reporter transcript decay, suggesting that RNA binding proteins like ARE-binding proteins and Pumilio may contribute to *her1* transcript degradation and help to maintain *her1* turnover during somitogenesis (Tietz et al., 2020).

Some RNA-binding proteins (RBPs) recruited by a specific cis-element, such as an ARE and/or PRE, recruit the degradation mechanism for transcript degradation (Pullmann et al, 2007). One class of RNA-binding proteins that promote transcript degradation when they bind 3'UTR AREs are ARE binding proteins (ARE-BPs) (Chou et al, 2006). For example, the RNA binding protein Zfp36l1 regulates neural induction and differentiation in *Xenopus* embryos by binding AU-rich elements in 3'UTR of target mRNAs and thus stimulating transcript turnover

(Xia et al, 2012). Another class of RNA binding proteins is the Pumilio proteins which play an important role in development. Pumilio proteins recognize the Pumilio Response element (PRE) and recruit the deadenylase complex to deadenylate and destabilize target transcripts (Brocard et al, 2018). By binding to the PRE on the *Gata6* 3'UTR, PUM1 decreased *Gata6* expression, which is essential for mouse embryo gastrulation (Lin et al, 2018).

Since previous studies indicated that the ARE and PRE are required for reporter transcript decay, I am analyzing the role of ARE and PRE on endogenous *her1* expression. I am using CRISPR/Cas9-mediated homology-directed repair (HDR) to introduce precise mutations in the ARE and PRE of the *her1* 3'UTR in zebrafish embryos. I will analyze how the PRE and ARE contribute to *her1* mRNA instability and whether changes in *her1* mRNA stability disrupt the *her1* period and impacts somitogenesis. My hypothesis is that ARE and PRE mutations in the *her1* 3'UTR will prevent binding of RBPs such as Pumilio and ARE-BPs, thus preventing recruitment of transcript degradation machinery and rapid *her1* mRNA decay. I predict that the resulting *her1* transcript accumulation will lead to increased *her1* protein levels, disrupting oscillatory *her1* expression, and leading to fused or disorganized somites.

Since homology-directed repair has very low efficiency, my mentor Monica Blatnik and I first tested the CRISPR knockout efficiency before attempting homology-directed repair. We reasoned that if CRISPR-induced mutagenesis efficiency was low, then HDR efficiency would be even lower. We tested knockout efficiency in wild-type zebrafish embryos. Following mutagenesis, we analyzed the general morphology of injected zebrafish embryos to see the impact of *her1* 3'UTR mutagenesis on somitogenesis and used in situ hybridization to monitor effects on *her1* and *myoD* expression. In future experiments, we will induce homologous recombination and precisely edit the ARE and PRE by injecting gRNAs targeting the *her1* 3'UTR and a DNA template containing mutated ARE and PRE sites, along with Cas9 protein into one-cell stage zebrafish embryos. We will then raise the injected zebrafish embryos and identify founder fish that contain the desired mutation using High-Resolution Melting Analysis (HRMA) and DNA sequencing. Finally, we will analyze molecular and morphological phenotypes in the mutated line. This will help us to study the mechanism of *her1* mRNA regulation and reveal the possible morphological changes caused by disrupted *her1* oscillatory expression.

Results:

Subcloning iSpyMac plasmid for in vitro transcription of *iSpyMac* mRNA.

To test the CRISPR/Cas9 system in mutating *her1* 3'UTR, we will design gRNA targeting ARE and PRE in *her1* 3'UTR, then inject the transcript of Cas9 and gRNA in one-cell stage zebrafish embryos, finally analyze the mutagenesis efficiency using HRMA.

Since 3'UTRs are generally A-T-rich, the standard Cas9 protein, which recognizes a 5'-NGG-3' protospacer adjacent motif (PAM) sequence, does not provide many options for gRNA target sequences near the *her1* 3'UTR ARE and PRE. The PAM is a short DNA sequence located downstream of the target DNA sequence that Cas9 nuclease recognizes to make a double-strand break (Mekler et al, 2020). The requirement for a 5'-NGG-3' PAM sequence limits the number of gRNA we are able to design in an A/T-rich 3'UTR using CHOPCHOP, an online tool used to design high-efficiency gRNAs to target a specified genomic region (ref). Since our final goal is to precisely mutate ARE and PRE using HDR, we need to choose gRNA which have high efficiency in incorporating mutation in ARE and PRE through HDR. A previous study indicates how the cut-to-mutation distance, the distance between incorporate mutation and Cas9 cut site, impacted HDR CRISPR/Cas9 mutagenesis efficiency in induced pluripotent stem cells (Paquet et al, 2016). The cut-to-mutation distance directly correlates with the efficiency of homozygous mutations, where shorter cut-to-mutation distances correlate with higher efficiency (Paquet et al, 2016). The efficiency is around 90% when the distance reached 0, and the efficiency is less than 30% when the distance is longer than 10bp. For heterozygous mutations, the efficiency is highest when the cut-to-mutation distance reached 10 bp, and the efficiency is close to zero when the cut-to-mutation distance surpasses 45 bp (Paquet et al, 2016). Thus, for efficient homology-directed repair in the *her1* 3'UTR, we need to minimize the cut-to-mutation distance, so we need to generate gRNAs that recognize targets closest to the ARE and PRE. Our gRNA target design was also limited by the requirement of the in vitro transcription enzyme we used, T7, which can only transcribe gRNAs starting with GG. Unfortunately, there was no gRNA available for Cas9 with the "NGG" PAM sequence that met all criteria.

To find an alternative method of altering A/T-rich sequences like the *her1* 3'UTR, we came across a study that engineered the SpyCas9 protein from the *Streptococcus pyogenes* bacterial strain (Chatterjee et al, 2020). iSpyMac is an engineered form of the SpyCas9 protein which has an altered PAM specificity from the standard "NGG" to "5'-NAAN-3'", the PAM sequence from the SmacCas9 protein from *Streptococcus macacae* (Chatterjee et al, 2020). Since iSpyMac Cas9 utilizes a 5'-NAAN-3' PAM, it would presumably function better on A-rich regions such as the *her1* 3' UTR. The efficiency of iSpyMac was tested in HEK293T cells, in which the modification rate of iSpyMac with most of the 5'-NAAN-3' PAM sequences reached over 40%, and the highest modification rate in the target sequence with a 5'-AAAA-3' PAM reached around 70% (Chatterjee et al, 2020).

The published iSpyMac plasmid contains an EF-1 alpha promoter for use in mammalian cells. Since the aim was to mutate the *her1* 3'UTR by injecting *iSpyMac* mRNA in zebrafish embryos, we needed to subclone the iSpyMac coding sequence to allow for in vitro transcription. By subcloning the iSpyMac Cas9 coding sequence in a $pCS2^{+}$ plasmid backbone, we were able to transcribe the iSpyMac Cas9 coding sequence. The EcoRI and Aval1 restriction enzymes were used to digest the iSpyMac plasmid, generating a 6kb fragment, a 2.2 kb fragment containing iSpyMac Cas9 coding region, and multiple smaller fragments outside of the Cas9 coding sequence (Fig. 1). $pCS2^{+}$ was digested by EcoRI and Aval1, generating a 4kb backbone that was ligated to the iSpyMac Cas9 coding fragment and transformed into bacteria (Fig. 1). The 4 kb $pCS2^{+}$ backbone we need cannot be separated from the $pCS2^{+}$ cutout fragment after being digested with EcoRl and Aval since the cutout fragment was too small to show up in the gel (Fig, 1). Therefore, the SAP enzyme was used to treat the $pcs2^{+}$ sample digested by EcoRI which prevented relegation of the $pcs2^{+}$ backbone and cutout fragment. The iSpyMac Cas9 fragment contained a 5' phosphate and 3' hydroxyl on each end after being digested by EcoRI and AvaI, and linearized $pcs2^{+}$ digested by EcoRI also contained a 5' phosphate and 3' hydroxyl on each end (Fig. 2, Fig. 3). SAP enzyme dephosphorylated the 5' phosphorylated ends of linearized $pcs2^{+}$ so that $pcs2^{+}$ contained 5' hydroxyl and 3' hydroxyl on both ends, then the linearized $pcs2^{+}$ was digested by AvaI, producing a backbone and a small cutout fragment (Fig. 2). In the $pcs2^{+}$ backbone and cutout fragment, the end digested by AvaI produced a 5' phosphate and 3' hydroxyl (Fig. 2). Another end with 5' hydroxyl and 3' hydroxyl prevented relegation of $pcs2^{+}$ backbone and its fragment (Fig. 2). The 5' phosphate on both end of the iSpyMac fragment allowed it to ligate with $pcs2^{+}$. However, a nick existed in subcloned plasmid since the 3' hydroxyl end of iSpyMac cannot ligate with the 5' hydroxyl end of $pcs2^{+}$, and this nick can be ligated after transformed in E.coli (Fig. 2).

After transforming the ligated plasmid into E.coli, independent clones were picked and grown in liquid culture. The plasmid was extracted, then was test digested using EcoRI and Aval to demonstrate it contained the correct fragment size we expected (Fig. 4). Then, we sequenced the inserted iSpyMac sequence to confirm the iSpyMac sequence matched the published sequence.

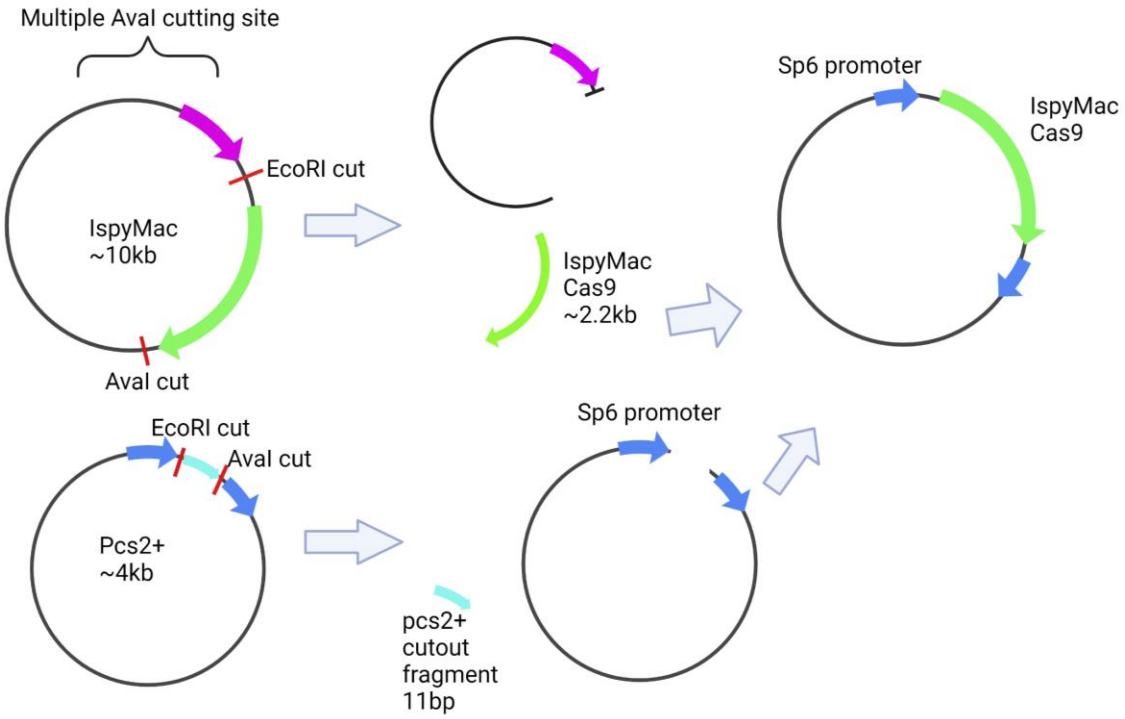

Figure 1.

iSpyMac subclone design

iSpyMac plasmid extracted from a single *E. coli* colony was digested with EcoRI and AvaI restriction enzymes and run on a gel to separate digested fragments. The iSpyMac Cas9 coding sequence was obtained through gel extraction. The pCS2^{+} plasmid extracted from single *E. coli* clone was digested with EcoRI and AvaI, then the plasmid backbone was extracted. The pCS2^{+} backbone and iSpyMac Cas9 coding sequence were ligated and transformed in *E.coli*.

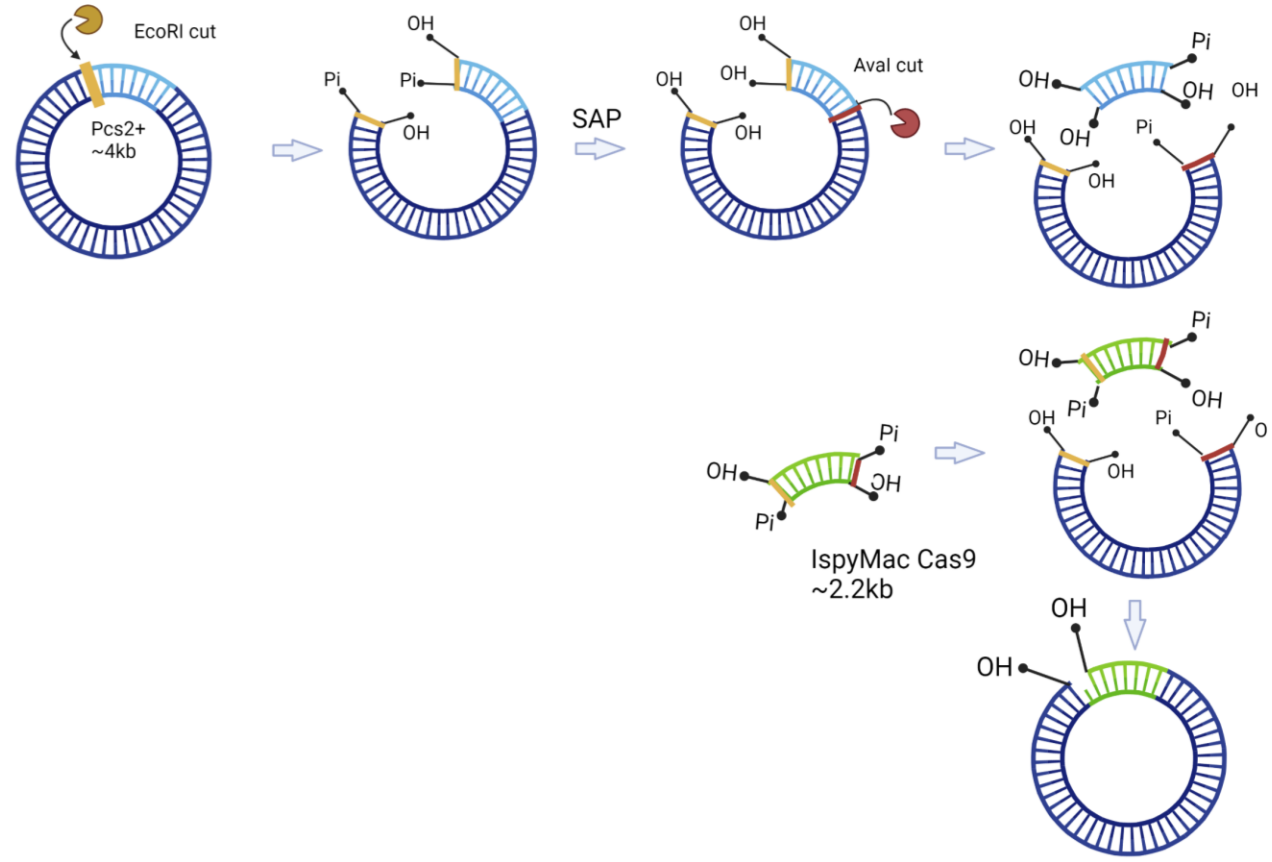

Figure 2.

pcs2^{+} SAP treatment

After being digested by EcoRI, each end of linearized pCS2^{+} contained 5' phosphate and 3' hydroxyl moieties. SAP enzyme dephosphorylates both 5' phosphate ends in pCS2^{+} fragment, leaving 5' hydroxyl and 3' hydroxyl ends. Then the linearized pCS2^{+} was digested by Aval, producing a 5' phosphate and 3' hydroxyl on the backbone (dark blue) and cutout fragment (light blue). The 5' hydroxyl and 3' hydroxyl end in pcs2^{+} fragment and backbone prevented them from relegation. Only iSpyMac Cas9 fragment which contained 5' phosphate on both ends should ligate with pCS2^{+} backbone and left a kink.

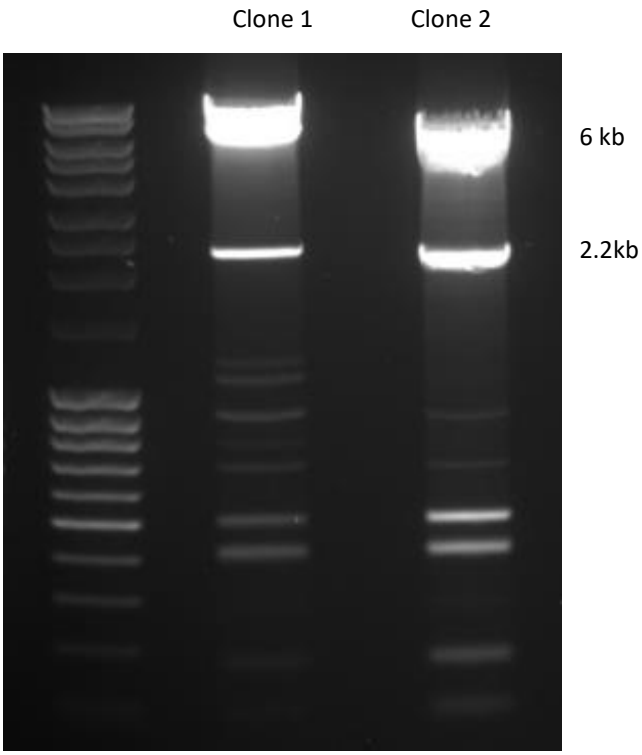

Figure 3.

iSpyMac plasmid gel image from independent clones digested with EcoRI and AvaI. The 2.2kb fragment corresponded to the Cas9 sequence. iSpyMac plasmid is 11 kb in size; after enzyme digestion, it produced a 6kb fragment, a 2.2 kb fragment, and multiple samller sized fragments that did not contain the iSpyMac coding sequence.

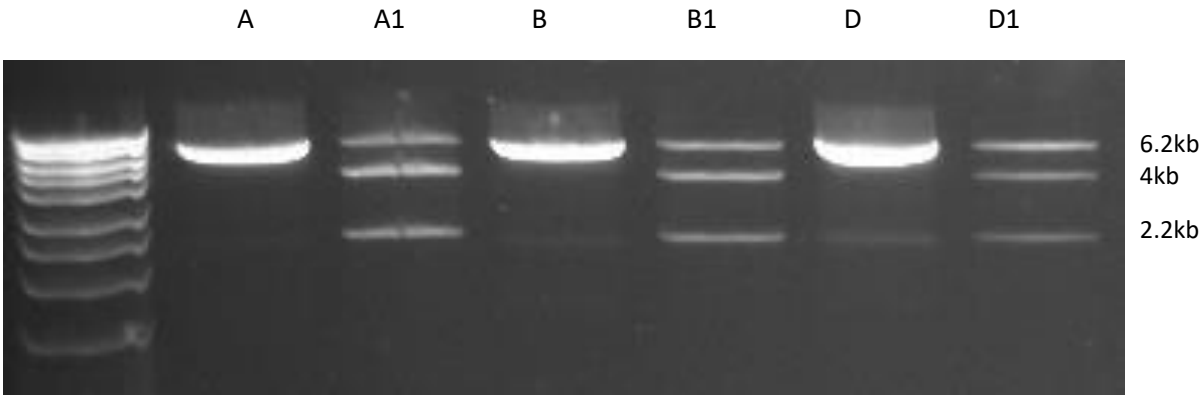

Figure 4.

Test digested subcloned plasmid with EcoRI and AvaI from independent clones. The subcloned iSpyMac plasmid generated a 6.2 kb fragment. Plasmid from each *E. coli* colony was digested with EcoRI and AvaI, generating a 2.2 kb fragment and a 4 kb fragment. The 6.2kb fragment corresponded to the undigested plasmid. A, B, C were the plasmids extracted from a single clone digested with EcoRI, which linarized the plasmid. A1, B1, C1 were the samples digested with both EcoRI and AvaI.

Microinjecting zebrafish embryos with *iSpyMac* mRNA and *her1* 3'UTR gRNAs failed to induce mutagenesis.

Although we designed several gRNA proximal to *her1* 3'UTR with iSpyMac, We were only able to in vitro transcribe one *her1* 3'UTR gRNA which naturally had a GG at the 5' end. We cannot in vitro transcribe the rest of gRNAs since they were started with "GA" or "GT" and the in vitro transcription enzyme T7 was only able to transcribe gRNA starting with GG. To in vitro transcribe gRNA starting with "GA" or "GT", we modified the synthesized RNA by adding a "G" at the 5' end where it did not contain a natural G. After transcribing our gRNAs and *iSpyMac* mRNA, we injected *iSpyMac* mRNA and gRNA targeting *her1* 3'UTR into one-cell stage zebrafish embryos, raised them to 24 hours post-fertilization (hpf) and genotyped the target region using High-Resolution Melt Analysis (HRMA). Using HRMA, sample DNA is amplified and fluorescent dye binds the double-stranded DNA. The sample DNA is then heated at high temperatures so that the DNA denatures, causing double-strand separation and the fluorescent dye fades. Fading of the dye generates a curve, which can be affected by a single base change. The curve can be used to detect minor base differences between wild-type and mutant alleles.

In the embryos analyzed by HRMA, 11 uninjected embryos were used as control, and 22 embryos were injected with *iSpyMac* transcript plus *her1* 3'UTR gRNA 4 or gRNA5 (Fig. 5, A). For the HRMA result of a successful mutation in injected embryos, I expected that all uninjected embryos would be located in one cluster and all injected embryos located in different clusters. The HRMA program detects the melt temperature difference in the target region of samples. If

the melt temperature difference was big enough, the program will put injected and uninjected embryos in distinct clusters with different colors, indicating that there was a mutation in an injected embryo. However, the HRMA result showed that all embryos clustered in the same green group, suggesting that there was no molecular difference between injected and uninjected embryos (Fig. 5A). We also injected embryos with *iSpyMac* mRNA and *her1* 3'UTR gRNA1, and we obtained a similar HRMA melt profile, where all injected and control embryos were located in the same cluster, suggesting mutations were not induced (data not shown). As a result, when using *iSpyMac* transcript and three different gRNAs that had a G added to the 5' end, none of the injected embryos showed evidence of induced mutations.

The added G on the 5' end of the gRNAs may have contributed to low mutagenesis efficiency. To test this, we used original gRNA without adding "G" on the 5'end. We discovered that the T7 enzyme was able to transcribe gRNAs starting with a single G, so we were able to use a gRNA starting with a single G. We used the original gRNA1 sequence without modification, and injected it with *iSpyMac* transcript in one-cell stage embryos. However, we still observed no indication of mutagenesis, based on the HRMA results (Fig. 5B). Therefore, when injecting *iSpyMac* transcript as the source for iSpyMac protein, using a gRNA that perfectly matches the target sequence does not appear to improve mutagenesis efficiency. However, as discussed later, there are several alternative explanations for this negative result.

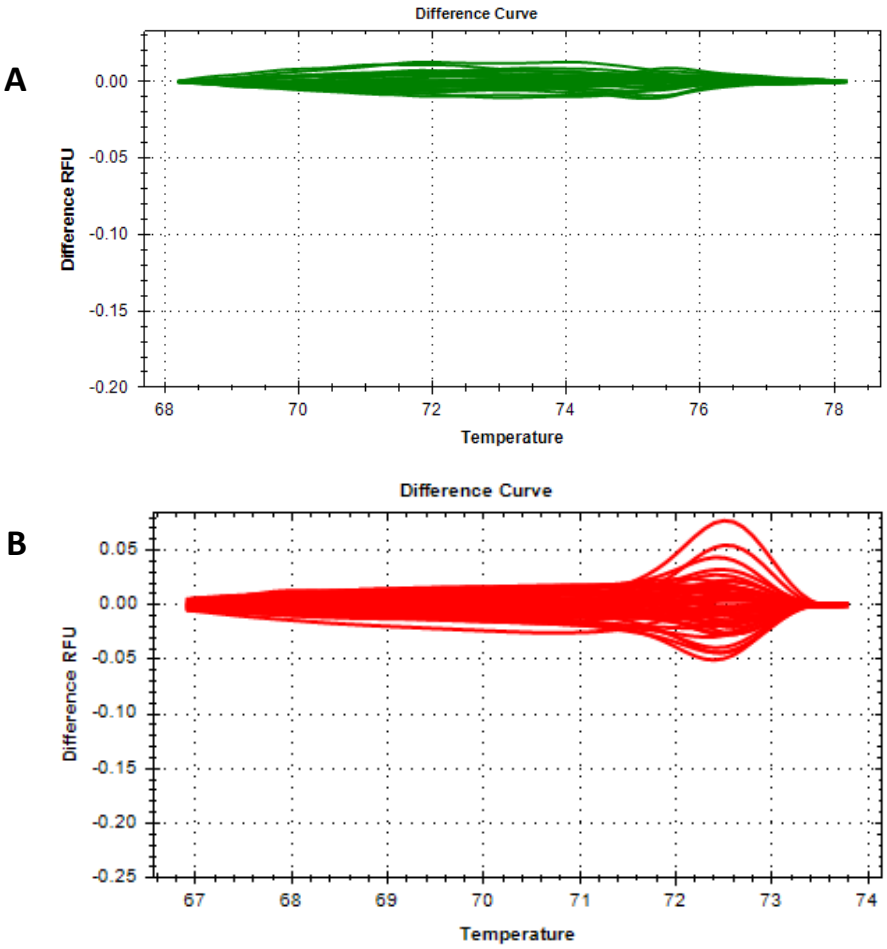

Figure 5.

HRMA genotype result of WT embryos injected with *iSpyMac* mRNA and *her1* 3'UTR gRNA with and without added "G" on 5'end

A: HRMA genotype result of wild-type embryos injected with *iSpyMac* mRNA and *her1* 3'UTR gRNA 4 or 5 with added "G" on 5' end. There were a total of 33 embryos in the green cluster, including 11 uninjected embryos, 9 embryos injected with gRNA 4 and *iSpyMac* transcript, 13 embryos injected with gRNA 5 and *iSpyMac* transcript. The HRMA result indicated that there was no difference in the melting temperature of the target DNA between injected and uninjected embryos, thus likely no mutagenesis.

B: HRMA genotype result of wild-type embryos injected with *iSpyMac* mRNA and origenal *her1* 3'UTR gRNA 1 wihout added "G" on 5'end. There were a total of 49 embryos in the red cluster, including 11 uninjected embryos and 38 injected embryos. The HRMA result indicated that there was no difference in the melting temperature of the target DNA between injected and uninjected embryos.

Injecting *iSpyMac* mRNA and gRNA targeting *rx3* gene failed to induce mutation in WT Zebrafish embryos.

Since we had targeted *her1* 3'UTR and did not see evidence of mutagenesis, it is possible that the *her1* 3'UTR is hard for Cas9 to locate and bind. Therefore, we decided to use iSpyMac to target *rx3*, a gene required for eye development that has been used as a proof of principle locus for many CRISPR/Cas9 systems (Hoshijima et al, 2019). Because we were not restricted to choose gRNAs targeting a specific location in the *rx3* coding sequence, we were able to design several gRNAs starting with G, so they could be transcribed by the T7 enzyme without requiring the 5' G addition.

We injected over 63 embryos and none showed the expected eyeless phenotype that is expected from complete loss of *rx3* function. Using HRMA to analyze 73 embryos, we observed that most of the *rx3* gRNA2 and *iSpyMac* transcript-injected embryos (n=62 of 63 total) clustered together with uninjected embryos (n=10 of 11 total) (see red cluster, Fig. 6). One uninjected embryo (n=1 of 11) and one injected embryo (n=1 of 63) showed a distinct melt profile (green cluster). However, we thought it unlikely that the differential melt profile of the injected embryo in the green cluster indicated successful targeted mutagenesis because an uninjected embryo showed a similar profile. We suspect that instead there is an SNP present in the population. Even if the locus was successfully targeted, the success rate (1/63) is very low, indicating very low efficiency. We also injected zebrafish embryos with *rx3* gRNA3 and gRNA7 and obtained a similar result, where both injected and uninjected embryos were located in the same cluster (data not shown).

HRMA results from several biological replicates and with multiple gRNAS suggested that mutations were not induced by injection of iSpyac Cas9-encoding transcript with targeting gRNAs. One possible explanation is that the *iSpyMac* Cas9 transcript is not properly translated into iSpyMac Cas9 protein. It is also possible that a mutation is induced which cannot be detected by HRMA. Most of the time various insertions and deletions are introduced in the target sequence as a result of random mutation after the Cas9 protein makes a double-strand break. HRMA is able to detect insertion and deletion, but if a mutation occurs that does not change the length of the target sequence, HRMA cannot detect it. However, the fact that we obtained the same result after using multiple gRNAs targeting *rx3* and the *her1* 3'UTR, it is unlikely that every introduced mutation would not be detected by HRMA. It is possible that the injected *iSpyMac* transcript is not properly translated or that the *iSpyMac* Cas9 protein does not function in zebrafish embryos. Taken together, our results indicate that injection of *iSpyMac* mRNA with various gRNAs into zebrafish embryos does not induce targeted mutagenesis.

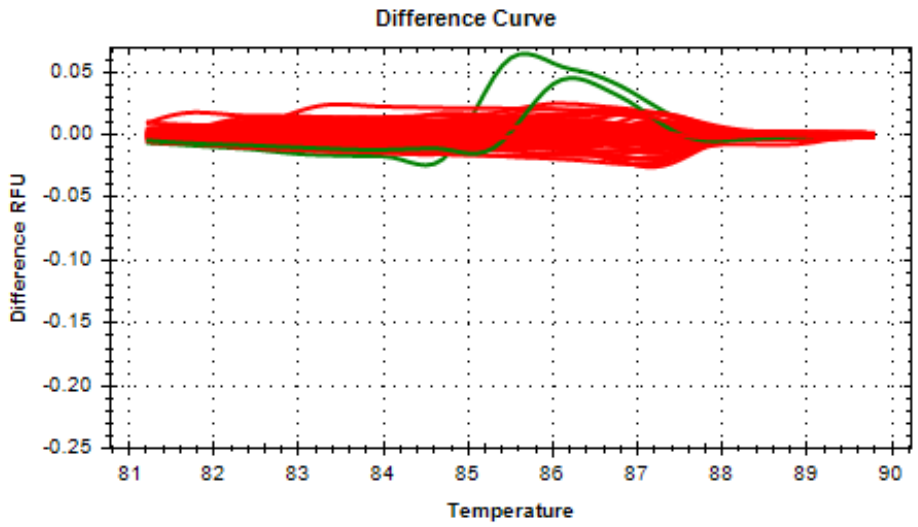

Figure 6.

HRMA genotype result of wild-type embryos injected with *iSpyMac* mRNA and *rx3* gRNA2.

Of 73 embryos total, 11 were uninjected embryos, and 63 were injected with *rx3* gRNA2 and *iSpyMac* mRNA. Most of the uninjected and injected embryos are in the red cluster. One injected embryo and one uninjected embryo are located in the green cluster. Same comment about "clusters" here.

Injecting Cas9 protein and gRNA targeting *her1* 3'UTR gene induced mutagenesis in WT Zebrafish embryos

Since we were unable to induce mutagenesis with the *iSpyMac* Cas9 system, we decided to inject recombinant Cas9 protein instead of *Cas9* mRNA. *S. pyogenes* Cas9 protein prefers a 5'-NGG-3' PAM sequence and has previously been shown to achieve high rates of mutagenesis in zebrafish embryos (Klatt et al., 2021). In a recent study that targeted 17 genes in zebrafish, mutagenesis efficiencies were above 85% when using Cas9 protein and chemically synthesized gRNAs (Klatt et al., 2021). Since the authors in the study purchased gRNA transcripts from a manufacturer, we also decided to purchase a chemically synthesized gRNA transcript. Moreover, by purchasing gRNA transcript, we were not limited to gRNAs starting with 5'G to satisfy the T7 polymerase requirement.

We chose a gRNA 9 bp upstream of PRE and ARE in *her1* 3'UTR based on the "NGG" target site and purchased the chemically synthesized gRNA transcript. *her1* gRNA 1 and Cas9 protein were injected into wild-type zebrafish embryos. There were 32 embryos in the first experiments, 11 uninjected and 21 injected embryos (Fig. 7A). When analyzed by HRMA, all

uninjected embryos had the same melt profile (green cluster) and served as the control group. Of 21 injected embryos, only 1 had a melt profile similar to the uninjected embryos; the other 20 injected embryos had a distinct profile (red cluster) (Fig. 7A). The large melt temperature deflection in injected embryos suggests successful mutagenesis. Based upon the HRMA results, we estimate that the mutagenesis rate was approximately 95% (20/21 embryos).

We performed a second experiment with a total of 56 embryos, 22 uninjected and 34 injected embryos (Fig. 7B). Of the 22 uninjected embryos analyzed by HRMA, 20 had similar melt profile (green cluster) and served as the control group and 2 had a distinct profile (pink cluster) (Fig. 7B). Of the 34 injected embryos, 31 embryos (red, orange, and blue clusters) had large melt temperature deflections compared to the control group, suggesting successful mutagenesis (Fig. 7B). There is also one injected embryo located in the neon green line. Only 2 uninjected embryos showed profiles like the control group (green cluster)(Fig. 7B). These results indicate that injecting Cas9 protein and synthesized gRNAs leads to much-improved mutagenesis rates, compared to the *iSpyMac* mRNA described earlier.

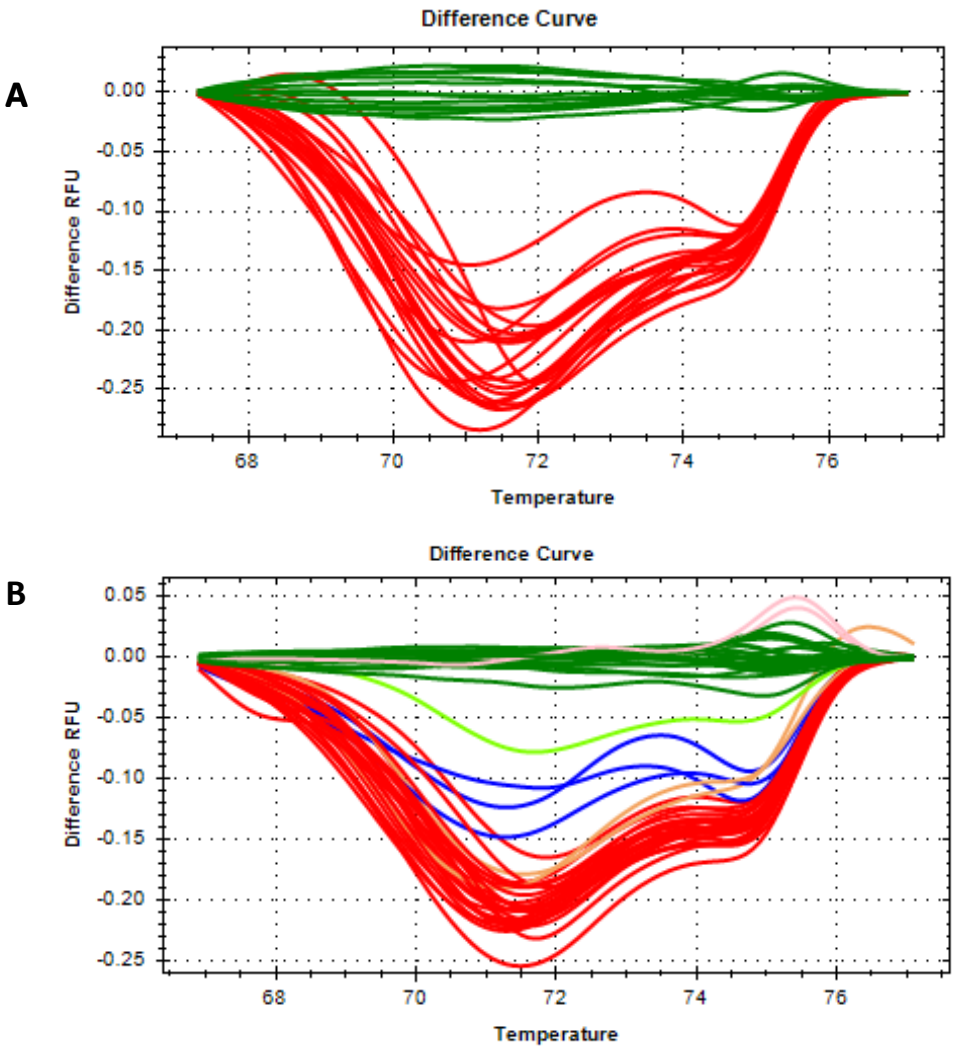

Figure 7.

HRMA reveals successful mutagenesis in embryos injected with Cas9 protein and *her1* 3'UTR gRNA

A: HRMA of zebrafish embryos injected with recombinant *S. pyogenes* Cas9 protein and *her1* 3'UTR synthesized gRNA. For this bioreplicate, a total of 32 embryos were analyzed. All 11 uninjected embryos showed a similar melt profile and clustered togther (green cluster) with only 1 injected embryos. Almost all injected embryos (20 of 21 total) had a different melt profile (red cluster).

B: HRMA of a bioreplicate experiment. A total of 56 embryos were analyzed after injection with recombinant *S. pyogenes* Cas9 protein and *her1* 3'UTR synthesized gRNA. The 22 uninjected embryos showed 2 distinct melt profiles, a majority in the green cluster (n=20) and fewer in the pink (n=2) cluster. All 34 injected embryos showed distinct profiles from uninjected embryos, with the majority (n=28) showing a strong deflection (red cluster). Additional profiles are revealed by the blue (n=3) and orange (n=2) clusters and the neon green line (n=1).

In-situ of embryos injected with *her1* 3'UTR gRNA and Cas9 protein has disrupted *her1* expression and *myoD* expression

After confirming mutagenesis through HRMA, we want to analyze how this mutation impacts her1 expression and somite development in the injected zebrafish embryo. F0 crispants, which are the wild-type embryos injected with *her1* 3'UTR gRNA and Cas9 protein, were raised to the mid-segmentation stage with uninjected embryos. Those embryos were fixed for in situ hybridization to analyze *her1* expression. In uninjected embryos, *her1* expression in PSM was regular and contained a clear *her1* expression boundary and striped *her1* expression (representative embryos shown in Fig. 7A). Of 6 injected embryos, we observed 4 embryos that had irregular *her1* expression patterns, and we choose F0 crispants#1 and #2 as representative embryos. In F0 crispant #1, *her1* expression was disrupted (Fig. 7B) and appeared in anterior PSM cells anterior to the PSM, which would normally lack *her1* expression in wild-type embryos (Fig. 7B). In F0 crispant #2, *her1* expression was irregular and asymmetric (Fig. 7C). These preliminary observations suggest that *her1* striped expression is disrupted in some F0 crispant embryos, suggesting that *her1* transcripts may be improperly regulated.

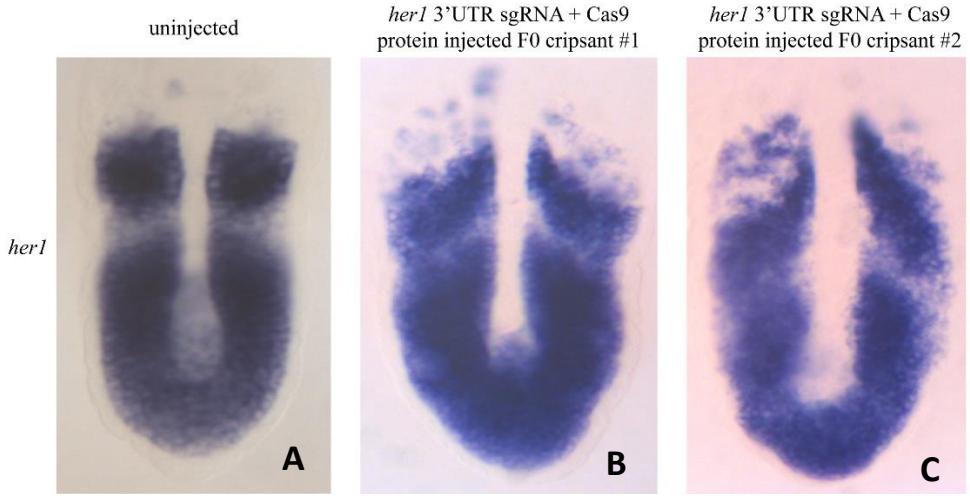

Figure 7.

In-situ hybridization for *her1* in uninjected control and *her1* 3'UTR gRNA and Cas9 protein-injected zebrafish embryos shows some . Dorso-posterior view of the PSM, anterior on top and posterior on the bottom. (A) A representative uninjected WT embryo shows normal, striped *her1* expression. Since *her1* expression is dynamic in the PSM, other control embryos show distinct patterns, usually with 2-3 "stripes" of expression. (B) F0 crispant #1 shows spotty *her1* expression anteriorly, in a region where *her1* expression would likely not be observed in a control embryo. (C) F0 cripsant #2 showed asymmetric *her1* expression across the midline.

After being injected with *her1* 3'UTR gRNA and Cas9 protein, the uninjected and injected embryos were raised to the mid-segmentation stage. Since the zebrafish embryos are transparent, it is hard to directly examine embryos' somites. Therefore, we fixed the embryo for in situ hybridization and analyze *myoD* expression, which marks the somites and adaxial cells (Zhang et al, 2006). Of 7 injected embryos, we observed 4 embryos that had disrupted *myoD* expression patterns. The uninjected embryo showed normal *myoD* expression which represented a clear somite pattern from anterior to posterior (Fig. 8, A). The F0 crispant #1 lost most of the *myoD* expression in somatic cells and only the adaxial cell *myoD* expression remained (Fig. 8, B). Small amounts of cells still remained *myoD* expression in somite, but there was no clear boundary and shape (Fig. 8, B). The F0 crispants #2 and #3 did not have clear boundaries between *myoD* expression on somites (Fig. 8, C, D). In certain parts of PSM, the *myoD* expression was diffused and lost a distinct shape. (Fig. 8, C, D). The posterior somites had an unclear boundary, and in the anterior, the boundary completely disappeared (Fig. 8, C, D). In the middle axis of F0 crispant #4, somites labeled by *myoD* expression appear fused with each other (Fig. 8, E).

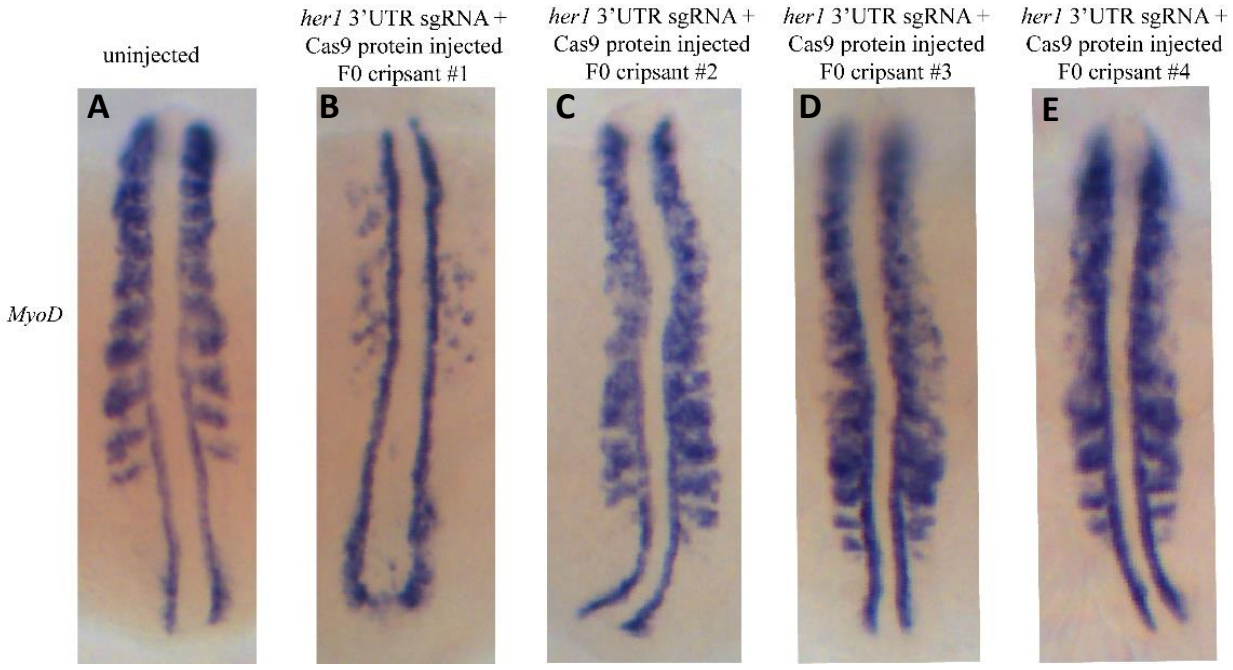

Figure 8.

In-situ hybridization for *myoD* expression in uninjected and *her1* 3'UTR gRNA and Cas9 protein-injected zebrafish embryos. Dorsal view, anterior on top posterior on the bottom. (A) The representative uninjected WT embryo shows normal *myoD* expression. (B) F0 crispant #1 had lost almost all *myoD* expression on somites, and adaxial cells remained *myoD* expression. (C,D) F0 crispants #2 and #3 did not have a clear boundary between *myoD* expression on somite, and the expression did not have a clear shape as shown in the uninjected embryo. (E) F0 crispant #4 had part of *myoD* expression loss in the middle of the anterior-posterior axis, and somites labeled by *myoD*

Discussion:

Attempts using iSpyMac transcript and in-vitro transcribed gRNA to induce mutations in zebrafish were unsuccessful

We injected wild-type one-cell stage embryos with *iSpyMac* transcript and multiple in vitro transcribed gRNAs (with and without added G on the 5' end) targeting the *her1* 3'UTR. Using HRMA, we did not observe evidence of mutation in injected embryos (Fig. 5A, B). We also injected embryos with *iSpyMac* transcript and multiple in vitro transcribed gRNA targeting *rx3,* a common "proof of principle" locus, and we still did not see the expected morphological phenotype (loss of eyes) or evidence of mutation using HRMA (Fig. 6). These results suggest that our attempts using *iSpyMac* transcript and in-vitro transcribed gRNAs failed to induce mutations in zebrafish. However, when we injected a synthesized *her1* 3'UTR gRNA and recombinant *S. pyogenes* Cas9 protein, we obtained estimated mutation rates of over 90% in injected embryos (estimates obtained via HRMA), indicating that this method achieves high-efficiency mutagenesis. In zebrafish F0 embryos (Fig. 7A, B), as expected from recently published work (Klatt et al., 2021).

There are several possible reasons why our *iSpyMac* approach did not work but our approach using recombinant *S. pyogenes* Cas9 protein and synthesized gRNA transcript was successful. One possible explanation is that the Cas9 protein with "NGG" PAM sequence preference functions better in zebrafish than iSpyMac protein, since iSpyMac is an engineered protein with altered PAM specificity, and iSpyMac was only tested in human cultured cells and in plants. It is also possible that injection of Cas9 protein achieves higher mutagenesis than Cas9 transcript, because there is no need for translation, allowing it to function earlier post-injection. It is also possible that the *iSpyMac* transcript is unstable after being injected into zebrafish or the transcript is inefficiently translated in zebrafish embryos. If the latter possibility is the case, then we could possibly bypass the issue by injecting iSpyMac protein to achieve successful mutagenesis. Finally, there could also be differences in the efficiencies of the two types of guide

RNAs used; the synthesized gRNA transcript may be more efficient than the in vitro transcribed gRNA.

her1 expression and *myoD* expression in embryos injected with Cas9 protein and *her1* 3'UTR gRNA were disrupted

We performed in-situ hybridization in injected embryos to see the impact of endogenous *her1* 3'UTR mutagenesis on *her1* and *myoD* expression. In WT embryos, *her1* and *myoD* expression are typically striped, with *her1* expressed in dynamic "stripes" in the PSM and myoD expressed in more persistent stripes in developing muscle cells in formed somites and the most anterior PSM. In F0 crispant embryos, *her1* expression was persistent in the anterior PSM which lacked *her1* expression in WT embryos. Some of the F0 crispant embryos (4/6 for *her1* and 4/7 for *myoD*) displayed abnormal *her1* or *myoD* expression (Fig. 7B, C. Fig. 8B- E). Although we did not confirm mutagenesis in the in situ embryos, the HRMA result from the other injected embryos showed that the rate of mutagenesis was over 90%, and part of the F0 crispant had a phenotype distinctive from uninjected embryos (4/6 for *her1* and 4/7 for *myoD*). Therefore, the high mutagenesis rates in both injection experiments suggested that the *her1* and *myoD* of F0 crispant embryos were very likely mutated.

There is variability in the phenotypes among the injected embryos, likely due to the nature of random mutations introduced in *her1* 3'UTR. This suggests that *her1* oscillation may be disturbed in injected embryo. Since *her1* 3'UTR mutation may disturb the protein binding site, it is possible that RNA binding proteins such as ARE binding proteins cannot be recruited and help to degrade the *her1* transcript. The accumulated *her1* may lead to continued *her1* expression, therefore the *her1* expression may fail to have a complete cycle. The *her1* in injected embryos also has persistent expression in the PSM anterior where no *her1* expression should exist. In F0 crispant #1, the persistent *her1* expression indicates that the accumulated *her1* transcript which may have a longer half-life in the cells at the time when it should be completely degraded.

myoD expression marks formed somites in wild-type embryos and the pattern appears disrupted in 4 of 7 F0 crispant embryos. In F0 crispant #2, only a few somite structures retained *myoD* expression (Fig. 8, B). It is possible that the mutagenesis increases the stability of *her1* transcript, and the accumulated *her1* transcript may translate into a high level of Her1 protein and strongly inhibits the *her1* expression. As result, the *her1* may not be able to oscillate, leading to a loss in *myoD* expression in somite. The F0 crispants #2, #3, and #4 have clear *myoD* expression boundaries in the posterior. However, in the middle and anterior axis, the boundary between *myoD* expression in somites disappeared. (Fig. 8, C, D, E). This probably indicates that the *her1* is not able to complete its oscillation cycle by stopping the *her1* expression in those mutants. The mutagenesis may lead to the accumulated *her1* transcript, and it is possible that

the stability of *her1* transcript is not so strong that it not will lead to a large loss of somite in *myoD* expression like the F0 crispants #1 (Fig. 8. B).

In summary, we were unable to induce mutagenesis in zebrafish embryos using *iSpyMac* system. However, we obtained high mutagenesis efficiency when using Cas9 protein and synthesized gRNA transcript. The mutation disrupts *her1* expression and *myoD* expression in F0 crispant embryos, which probably leads to *her1* transcript accumulation and loss of striped expression pattern in *her1* and *myoD*. This supports the hypothesis that sequences in the *her1* 3'UTR are important in endogenous *her1* post-transcriptional regulation and somitogenesis. In the future, we will use homology-directed repair to introduce precise mutations in the *her1* 3'UTR ARE and PRE in the wildtype zebrafish embryo, then analyze how precisely mutated ARE and PRE impact *her1* expression and somitogenesis.

Materials and Methods:

Subclone iSpyMac:

We purchased the iSpyMac plasmid from Addgene, originally published in Chatterjee et al, 2020. iSpyMac and pcs2^{+} were digested with EcoRI and ran on TAE gel. Linearized iSpyMac and pcs2^{+} were obtained using a gel recovery kit. Linearized iSpyMac was digested with AvaI and ran on a TAE gel. iSpyMac Cas9 coding region was obtained using a Gel recovery kit. Linearized pcs2^{+} was treated with SAP enzyme, then the reaction was cleaned using a gel recovery kit, followed by digestion with AvaI. The pcs2^{+} backbone was ligated with iSpyMac coding fragment using T4 DNA ligase from the NEB Quick Ligase kit and transformed into E.coli cells. Subcloned plasmids from independent colonies were extracted using a Mini-prep plasmid DNA purification kit. The subcloned iSpyMac plasmid was linearized, then the linearized subcloned iSpyMac was in vitro transcribed using SP6 enzyme to obtain *iSpyMac* mRNA. The gene-specific gRNAs were amplified using PCR, then the amplicon was in vitro transcribed using the T7 enzyme. The synthesized *iSpyMac* and gRNA transcript were purified using an RNA purification kit. The gRNA transcript was run on a gel to confirm its size.

Microinjection:

For *iSpyMac* mRNA and in vitro transcribed gRNA microinjections, we mixed one single gRNA and *iSpyMac* mRNA in a tube on ice, then injected the mixture into one-cell stage zebrafish embryos. A total of 400 ng of gRNA and 800 ng of *iSpyMac* transcript were added to a 10 ul injection mix. Then we raised embryos to 24hpf and genotyped the target region using High-Resolution Melt Analysis (HRMA).

For recombinant *S. pyogenes* Cas9 protein injection, we used diluted Cas9 protein in 25 uM and obtained synthesized gRNA transcript from IDT at 100 uM (Klatt Shaw and Mokalled, 2021). Equal volumes of 25uM Cas9 protein and 25uM *her1* sgRNA were mixed together for microinjections.

In situ:

In situ hybridization was performed by following the previous protocol. (Broadbent and Read, 1999; Jowett, 1998) Anti-DIG secondary antibodies were used for calorimetric in situ.

HRMA:

We performed HRMA to genotype embryos using Precision Melt Supermix for High-Resolution Melt (HRM) Analysis from BioRad, water, *her1* 3'UTR HRM F2, and *her1* 3'UTR HRM R2. For *rx3* gRNA 2 HRMA, we used water, Precision Melt Supermix for High-Resolution Melt (HRM) Analysis, *rx3* HRM F4 and R4. For *rx3* gRNA 3 and *rx3* gRNA 7 HRMA, we used water, Precision Melt Supermix for High-Resolution Melt (HRM) Analysis, *rx3* HRM F6 and R6.

Table for gRNA and primer

	sequence
her1 3'UTR gRNA1	GTCTTTCTTTTTTCCTATGGTAAA
her1 3'UTR gRNA1 with added "G" on 5'end	GGTCTTTCTTTTTTCCTATGGTAAA
her1 3'UTR gRNA4 with added "G" on 5'end	GGTACAGTTTTTTCACTTATTAAAA
her1 3'UTR gRNA5 with added "G" on 5'end	GGTACAGTTTTTTCACTTATTAAA
rx3 gRNA2	GGGCCGGTCAACCAGGGCTCTAAC
rx3 gRNA3	GGCGTTTCCATATGGATCGGGAAA
rx3 gRNA7	GCGTTTCCATATGGATCGGGAAAG
her1 3'UTR HRM F	GTGTTCTGGGGTCTTTGCTG
her1 3'UTR HRM R	CAATTAATTTACAATCTACAAAAGGTAG
rx3 HRM F4	AACGAGGATCCACAGCATTG
rx3 HRM R4	ACAAGTGCTCGGTGTCTTTG
rx3 HRM F6	TCCATCAAGCTGCAGGAGTC
rx3 HRM R6	TGATGAAGCTGGGCAGAGATTG

her1 3'UTR gRNA1 for Cas9 protein injection	ATGGTAAATTCTTTATTGTT

References

1. Brocard, Michèle et al. "Pumilio directs deadenylation-associated translational repression of the cyclin-dependent kinase 1 activator RGC-32." *Nucleic acids research* vol. 46,7 (2018): 3707-3725. doi:10.1093/nar/gky038

2. Broadbent J, Read EM, 1999. Wholemount in situ hybridization of Xenopus and zebrafish embryos. *Methods in molecular biology* 127, 57–67.

3. Bessho, Y et al. "Dynamic expression and essential functions of Hes7 in somite segmentation." *Genes & development* vol. 15,20 (2001): 2642-7. doi:10.1101/gad.930601

4. Choorapoikayil, Suma et al. "Analysis of her1 and her7 mutants reveals a spatio temporal separation of the somite clock module." PloS one vol. 7,6 (2012): e39073. doi:10.1371/journal.pone.0039073

5. Chou, Chu-Fang et al. "Tethering KSRP, a decay-promoting AU-rich element-binding protein, to mRNAs elicits mRNA decay." *Molecular and cellular biology* vol. 26,10 (2006): 3695-706. doi:10.1128/MCB.26.10.3695-3706.2006

6. Chatterjee, Pranam et al. "A Cas9 with PAM recognition for adenine dinucleotides." *Nature communications* vol. 11,1 2474. 18 May. 2020, doi:10.1038/s41467-020-16117-8

7. Dawson, S R et al. "Specificity for the hairy/enhancer of split basic helix-loop-helix (bHLH) proteins maps outside the bHLH domain and suggests two separable modes of transcriptional repression." *Molecular and cellular biology* vol. 15,12 (1995): 6923-31. doi:10.1128/MCB.15.12.6923

8. Giudicelli, François et al. "Setting the tempo in development: an investigation of the zebrafish somite clock mechanism." *PLoS biology* vol. 5,6 (2007): e150. doi:10.1371/journal.pbio.0050150

9. Gomez, Céline et al. “Control of segment number in vertebrate embryos.” *Nature* vol. 454,7202 (2008): 335-9. doi:10.1038/nature07020

10. Gallagher, Thomas L et al. “Pnrc2 regulates 3'UTR-mediated decay of segmentation clock-associated transcripts during zebrafish segmentation.” *Developmental biology* vol. 429,1 (2017): 225-239. doi:10.1016/j.ydbio.2017.06.024

11. Gajewski, Martin et al. “Anterior and posterior waves of cyclic her1 gene expression are differentially regulated in the presomitic mesoderm of zebrafish.” *Development* (Cambridge, England) vol. 130,18 (2003): 4269-78. doi:10.1242/dev.00627

12. Herrgen, Leah et al. “Intercellular coupling regulates the period of the segmentation clock.” *Current biology : CB* vol. 20,14 (2010): 1244-53. doi:10.1016/j.cub.2010.06.034

13. Hoshijima, Kazuyuki et al. “Highly Efficient CRISPR-Cas9-Based Methods for Generating Deletion Mutations and F0 Embryos that Lack Gene Function in Zebrafish.” *Developmental cell* vol. 51,5 (2019): 645-657.e4. doi:10.1016/j.devcel.2019.10.004

14. Jowett T, 1998. Analysis of protein and gene expression. *Methods in Cell Biology* 59, 63–85.

15. Kageyama, Ryoichiro et al. “Oscillatory gene expression and somitogenesis.” Wiley interdisciplinary reviews. *Developmental biology* vol. 1,5 (2012): 629-41. doi:10.1002/wdev.46

16. Klatt Shaw, Dana, and Mayssa H Mokalled. “Efficient CRISPR/Cas9 mutagenesis for neurobehavioral screening in adult zebrafish.” *G3 (Bethesda, Md.)* vol. 11,8 (2021): jkab089. doi:10.1093/g3journal/jkab089

17. Lin, Kaibo et al. “Essential requirement of mammalian Pumilio family in embryonic development.” *Molecular biology of the cell* vol. 29,24 (2018): 2922-2932. doi:10.1091/mbc.E18-06-0369

18. Mekler, Vladimir et al. “Quantification of the affinities of CRISPR-Cas9 nucleases for cognate protospacer adjacent motif (PAM) sequences.” *The Journal of biological chemistry* vol. 295,19 (2020): 6509-6517. doi:10.1074/jbc.RA119.012239

19. Pais-de-Azevedo, Tomás et al. “Recent advances in understanding vertebrate segmentation.” *F1000Research* vol. 7 97. 23 Jan. 2018, doi:10.12688/f1000research.12369.1

20. Palmeirim, I et al. “Avian hairy gene expression identifies a molecular clock linked to vertebrate segmentation and somitogenesis.” *Cell* vol. 91,5 (1997): 639-48. doi:10.1016/s0092-8674(00)80451-1

21. Pullmann, Rudolf Jr et al. “Analysis of turnover and translation regulatory RNA-binding protein expression through binding to cognate mRNAs.” *Molecular and cellular biology* vol. 27,18 (2007): 6265-78. doi:10.1128/MCB.00500-07

22. Paquet, Dominik et al. “Efficient introduction of specific homozygous and heterozygous mutations using CRISPR/Cas9.” *Nature* vol. 533,7601 (2016): 125-9. doi:10.1038/nature17664

23. Xia, Ying-Jie et al. “Involvement of XZFP36L1, an RNA-binding protein, in Xenopus neural development.” *Dong wu xue yan jiu = Zoological research* vol. 33,E5-6 (2012): E82-8. doi:10.3724/SP.J.1141.2012.E05-06E82

24. Zhang, Yuqing et al. “Characterization of muscle-regulatory gene, MyoD, from flounder (Paralichthys olivaceus) and analysis of its expression patterns during embryogenesis.” *Marine biotechnology (New York, N.Y.)* vol. 8,2 (2006): 139-48. doi:10.1007/s10126-005-5042-0